Int. J. Heat Mass Transfer. Vol. 15, pp. 801–817. Pergamon Press 1972. Printed in Great Britain

HEAT AND MASS TRANSFER PHENOMENA FOR VISCOUS FLOW IN CURVED CIRCULAR TUBES

C. E. KALB and J. D. SEADER

Department of Chemical Engineering, University of Utah, Salt Lake City, Utah, U.S.A.

(*Received* 10 *May* 1971 *and in revised form* 12 *August* 1971)

Abstract—Heat transfer to steady viscous flow in curved tubes of circular cross section was studied theoretically for fully developed velocity and temperature fields under the thermal boundary condition of axially uniform wall heat flux with peripherally uniform wall temperature. The fully developed velocity profiles utilized were calculated by means of a rigorous numerical method [1]. The thermal-energy equation was solved numerically by use of a point successive-overrelaxation method. Results are not limited to slightly curved tubes and low Dean numbers, as in previous analyses. Solutions are presented for a Dean-number range from 1 to 1200. Prandtl-number and curvature-ratio parameters varied from 0·005 to 1600 and from 10 to 100, respectively. The peripherally averaged Nusselt number could be correlated as a function of Dean and Prandtl numbers only; but, when peripheral variation of the Nusselt number is considered, the curvature ratio enters as an additional parameter.

NOMENCLATURE

a, inside radius of tube;
A, area of inside surface of tube;
c_p, specific heat at constant pressure;
D, diffusivity of a diffusing substance in the fluid;
De, Dean number $\equiv Re(a/R)^{\frac{1}{2}}$;
f, Fanning friction factor $\equiv 2\bar{\tau}_w/(\rho w_m^2) = (-4/Re^2)(\partial P/\partial Z)$;
h, local heat-transfer coefficient $\equiv q/(T_w - T_m)$;
$\bar{h}$, peripherally averaged heat-transfer coefficient $\equiv \bar{q}/(T_w - T_m)$;
H, dimensionless temperature $\equiv (T_w - T)(R/a)/(Re\,Pr\,\mathrm{d}T_m/\mathrm{d}\psi)$;
H_m, flow-averaged dimensionless temperature;
k, thermal conductivity;
Nu, local Nusselt number $\equiv 2ha/k$;
$\overline{Nu}$, peripherally averaged Nusselt number $\equiv 2\bar{h}a/k$;
p, pressure;
P, dimensionless pressure $\equiv pa^2/\rho\nu^2$;
$\partial P/\partial Z$, dimensionless axial-pressure gradient $\equiv (\partial P/\partial\psi)/(R/a)$, constant;
Pr, Prandtl number $\equiv \nu/\alpha$;
q, local heat flux at the wall;
$\bar{q}$, peripherally averaged heat flux at at the wall, constant;
r, radial coordinate in the tube cross section;
R, radius of curvature of the tube at the center line;
R/a, curvature-ratio parameter;
Re, Reynolds number $\equiv w_m 2a/\nu$;
Sc, Schmidt number $\equiv \nu/D$;
T, local temperature;
T_m, flow-averaged mean temperature;
T_w, wall temperature;
u, v, w, velocity components in r, θ, ψ directions, respectively;
U, V, W, dimensionless velocity components in η, θ, ψ directions, respectively;
w_m, average velocity in ψ direction;
z, axial distance along tube center line, $R\psi$;

Z, dimensionless axial distance $\equiv z/a$.

Greek symbols

α, thermal diffusivity $\equiv k/(\rho c_p)$;
ε, convergence criterion;
η, dimensionless radial coordinate $\equiv r/a$;
θ, angular coordinate in the tube cross section;
μ, viscosity;
ν, kinematic viscosity $\equiv \mu/\rho$;
ρ, density;
τ_w, shear stress at the wall;
ϕ, dimensionless temperature $= (T_w - T)/(T_w - T_m) = H/H_m$;
ψ, angular coordinate normal to the tube cross section;
ω, relaxation factor.

Subscripts

1, 2, two axial positions, ψ_1 and ψ_2;
c, curved tube, also critical value;
I, J, indices used in numerical solution;
i, value at inner wall ($\theta = -\pi/2$);
m, flow-averaged mean value;
o, value at outer wall ($\theta = +\pi/2$);
s, straight tube;
w, value at wall.

Superscripts

—, peripherally averaged value;
n, nth iteration.

INTRODUCTION

CURVED tubes are employed in many important heat-transfer applications. Recently, interest has been expressed in increasing mass-transfer rates in membrane blood oxygenators [2] and in artificial kidneys [3] by use of secondary flows such as those induced by curved-tube flow channels. Knowledge of the variation in transport properties around the cross section of a curved tube can offer advantages in instances where the entire curved surface is not being utilized for boundary transport.

Dean [4, 5] was the first to predict theoretically secondary flow caused by centrifugal forces His perturbation analysis predicted that, for large curvature ratios (R/a), the friction loss was a function of a single parameter, which is now called the Dean number ($De \equiv Re\sqrt{a/R}$). Topakoglu [6] presented a perturbation solution which showed a small dependence on the curvature parameter over that expressed in the Dean number. These perturbation solutions are limited to very low Dean numbers. In the high-Dean-number region, approximate boundary-layer solutions for the velocity profiles were obtained by Adler [7], Barua [8], and Mori and Nakayama [9]. Truesdell and Adler [10] solved numerically the continuity and Navier–Stokes equations for Dean numbers as large as 200.

Recently, Austin [1] calculated fully developed velocity profiles numerically for Dean numbers from 1 to 1000 and curvatures from 5 to 100. His calculated friction factors are in good agreement with experimental measurements. In addition, Austin measured the axial-velocity component for air flow and found good

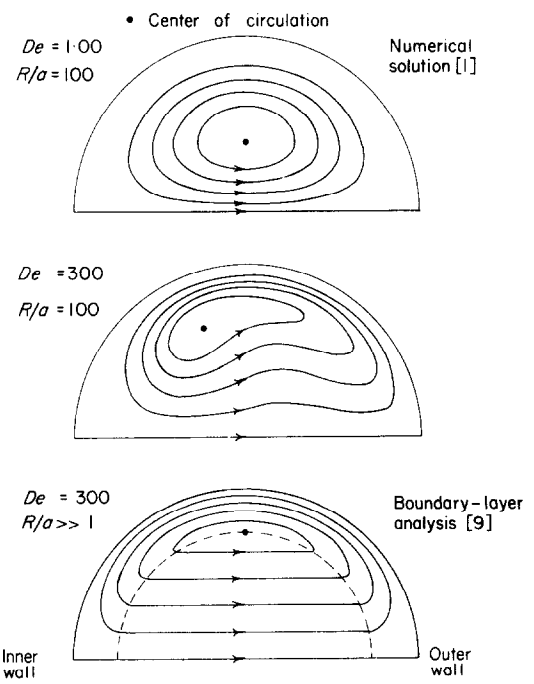

FIG. 1. Comparison of secondary-flow streamlines.

agreement with his numerical results. He concluded that, although the boundary-layer solutions are sufficiently accurate to predict curved-tube friction factors, the assumed secondary-flow field used in those analyses was oversimplified. Figure 1 shows Austin's calculated secondary-flow streamlines for Dean numbers of 1 and 300, characteristic of the low- and high-Dean-number regions, respectively. Mori and Nakayama's [9] boundary-layer results for a Dean number of 300 are also shown. The boundary-layer assumption of a uniform secondary flow in the central region and the location of the center of circulation are seen to differ from the numerical solutions. Austin's solution for the fully developed velocity profiles was used in this study of the heat-transfer problem.

Because curved-tube heat transfer is not axially symmetric, the nature of the bounding surface must be considered carefully. Two boundary conditions often considered are constant wall temperature and axially uniform wall heat flux with peripherally uniform wall temperature at each axial position. This study is concerned with the latter boundary condition; and, unless specifically noted, it will be referred to simply as the "constant-heat-flux condition".

Hawes [11] was the first to report measurements of fully developed temperature profiles in curved tubes. His data for water showed that temperature profiles were markedly different from those obtained in straight tubes and that the local heat-transfer coefficient at the outer wall was greater than that at the inner wall.

Seban and McLaughlin [12] measured local heat-transfer coefficients for an oil. They observed that the wall temperature varied peripherally but could not accurately account for the heat conducted peripherally in the wall, making the exact nature of their experimental boundary condition uncertain. They observed that the thermal entrance length was much shorter than that required for straight tubes.

Mori and Nakayama obtained the first theoretical heat-transfer solutions by boundary-layer methods for the constant-heat-flux [9] and constant-wall-temperature [13] boundary conditions, concluding that, to a first approximation, the asymptotic Nusselt number was independent of the two boundary conditions studied and that the Nusselt number became proportional to the 0·5 power of the Dean number at very large Dean numbers. It is shown by Dravid *et al.* [14], however, that Mori and Nakayama's Prandtl-number dependence is inaccurate. For $Pr > 1$, Mori and Nakayama [9, 13] integrated the energy integrals of the thermal boundary layer over the hydrodynamic boundary layer rather than over the thermal boundary layer.

Perturbation solutions of the thermal-energy equation at low Dean numbers have been presented. Özisik and Topakoglu [15] considered axially uniform wall heat flux with peripherally uniform wall temperature. Maekawa [16] studied both uniform wall temperature and axially and peripherally uniform wall heat flux.

Dravid *et al.* [14] obtained a numerical solution for entrance-region heat transfer in curved tubes using the fully developed velocity profiles developed by Mori and Nakayama [9]. Several boundary conditions were investigated, and results are presented for a single Dean number of 225. Their numerical solutions predicted that the local Nusselt number is an oscillatory function of increasing downstream distance. The oscillations, which were explained by considering the time delay for the secondary flow to pass across the central region of the tube, damp out as the region of the fully developed temperature field is approached. Dravid *et al.* also made measurements of the local, peripherally averaged Nusselt number using an electrically heated coil. They also confirmed the early convergence to the fully developed region first discovered by Seban and McLaughlin [12].

The study reported here is based on a numerical solution of the constant-property continuity, Navier–Stokes, and thermal-energy equations. Results for the boundary condition of axially uniform wall heat flux with peripherally uniform wall temperature are presented for Dean num-

bers of 1–1200, Prandtl numbers of 0·005–1600, and curvatures of 10–100.

FORMULATION OF THE PROBLEM

An orthogonal, toroidal coordinate system (r, θ, ψ) is depicted in Fig. 2, where R is the radius of the center line of the curved tube and a is the inside radius of the tube. This coordinate system is approximated by helical coils of small pitch, where pitch is the lateral displacement of successive turns of the coil. Velocities in the r, θ and ψ directions are u, v and w, respectively.

The following dimensionless quantities are defined:

$$\eta = \frac{r}{a},\ Z = \frac{z}{a},\ P = \frac{a^2 p}{\rho \nu^2},\ U = \frac{ua}{\nu},\ V = \frac{va}{\nu},\ W = \frac{wa}{\nu}, \quad (1)$$

where z is the axial distance along the tube center line ($z = R\psi$), p is the pressure, ρ is the density, and ν is the kinematic viscosity. When applied to the coordinate system of Fig. 2 and cast in terms of the dimensionless quantities defined above, the continuity and Navier–Stokes equations for steady, fully developed viscous flow of a constant-property fluid assume the form:

Continuity

$$\frac{\partial U}{\partial \eta} + \frac{U}{\eta} + \frac{U \sin\theta}{R/a + \eta \sin\theta} + \frac{1}{\eta}\frac{\partial V}{\partial \theta} + \frac{U \sin\theta}{R/a + \eta \sin\theta} = 0; \quad (2a)$$

η-component

$$U\frac{\partial U}{\partial \eta} + \frac{V}{\eta}\frac{\partial U}{\partial \theta} - \frac{V^2}{\eta} - \frac{W^2 \sin\theta}{R/a + \eta \sin\theta} = -\frac{\partial P}{\partial \eta} + \frac{\partial^2 U}{\partial \eta^2} + \left(\frac{\sin\theta}{R/a + \eta \sin\theta} + \frac{1}{\eta}\right)\frac{\partial U}{\partial \eta} - \left(\frac{\sin^2\theta}{(R/a + \eta \sin\theta)^2} + \frac{1}{\eta^2}\right)U + \frac{1}{\eta^2}\frac{\partial^2 U}{\partial \theta^2} + \frac{\cos\theta}{\eta(R/a + \eta \sin\theta)}\frac{\partial U}{\partial \theta} - \frac{2}{\eta^2}\frac{\partial V}{\partial \theta} - \frac{\cos\theta}{R/a + \eta \sin\theta}\left(\frac{\sin\theta}{R/a + \eta \sin\theta} + \frac{1}{\eta}\right)V; \quad (2b)$$

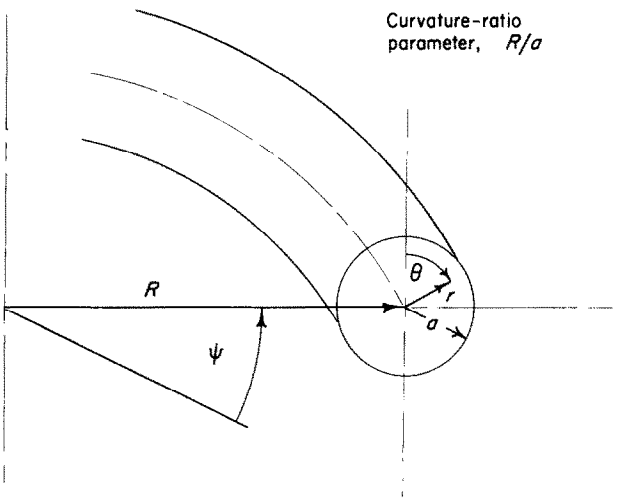

FIG. 2. Toroidal coordinate system for a curved circular tube.

θ-component

$$U\frac{\partial V}{\partial \eta} + \frac{UV}{\eta} + \frac{V}{\eta}\frac{\partial V}{\partial \theta} - \frac{W^2 \cos\theta}{R/a + \eta \sin\theta} = -\frac{1}{\eta}\frac{\partial P}{\partial \theta} + \frac{\partial^2 V}{\partial \eta^2} + \left(\frac{\sin\theta}{R/a + \eta \sin\theta} + \frac{1}{\eta}\right)\frac{\partial V}{\partial \eta}$$

$$-\left(\frac{\cos^2\theta}{(R/a+\eta\sin\theta)^2}+\frac{1}{\eta^2}\right)V+\frac{1}{\eta^2}\frac{\partial^2 V}{\partial\theta^2}+\frac{\cos\theta}{\eta(R/a+\eta\sin\theta)}\frac{\partial V}{\partial\theta}+\frac{2}{\eta^2}\frac{\partial U}{\partial\theta}+\frac{(R/a)\cos\theta\cdot U}{\eta(R/a+\eta\sin\theta)^2}; \quad (2c)$$

ψ-component

$$U\frac{\partial W}{\partial\eta}+\frac{V}{\eta}\frac{\partial W}{\partial\theta}+\frac{(U\sin\theta+V\cos\theta)W}{R/a+\eta\sin\theta}=-\frac{R/a}{R/a+\eta\sin\theta}\frac{\partial P}{\partial Z}+\frac{\partial^2 W}{\partial\eta^2}+\left(\frac{\sin\theta}{R/a+\eta\sin\theta}+\frac{1}{\eta}\right)\frac{\partial W}{\partial\eta}-\frac{W}{(R/a+\eta\sin\theta)^2}+\frac{1}{\eta^2}\frac{\partial^2 W}{\partial\theta^2}+\frac{\cos\theta}{\eta(R/a+\eta\sin\theta)}\frac{\partial W}{\partial\theta}, \quad (2d)$$

where $\partial P/\partial Z$ is a dimensionless, constant, axial-pressure gradient along the center line of the tube.

Equations (2) were solved by Austin [1] by introducing a stream function for the secondary velocities and the definition of vorticity. A set of three simultaneous, second-order, nonlinear, elliptic partial-differential equations in stream function, axial velocity, and axial component of vorticity were obtained, which were solved by a point successive-overrelaxation method. A full discussion of the method and its results is given by Austin [1].

The dimensional thermal-energy equation for steady-state viscous flow of a constant-property fluid through a circular curved tube, when viscous dissipation is neglected, is

$$u\frac{\partial T}{\partial r}+\frac{v}{r}\frac{\partial T}{\partial\theta}+\frac{w}{R+r\sin\theta}\frac{\partial T}{\partial\psi}=\frac{\nu}{Pr}\left(\frac{\partial^2 T}{\partial r^2}+\frac{1}{r}\frac{\partial T}{\partial r}+\frac{\sin\theta}{R+r\sin\theta}\frac{\partial T}{\partial r}+\frac{1}{r^2}\frac{\partial^2 T}{\partial\theta^2}+\frac{\cos\theta}{r(R+r\sin\theta)}\frac{\partial T}{\partial\theta}+\frac{1}{(R+r\sin\theta)^2}\frac{\partial^2 T}{\partial\psi^2}\right). \quad (3)$$

For transport processes in curved circular tubes, allowance must be made for proper averaging of certain quantities around the tube periphery. The surface area between any two axial positions, ψ_1 and ψ_2, is given by

$$A=\int_0^{2\pi}\int_{\psi_1}^{\psi_2}(R+a\sin\theta)a\,d\psi\,d\theta=2\pi aR(\psi_2-\psi_1). \quad (4)$$

The area-averaged value of the local wall heat flux, for example, for any region of the tube is then given by

$$\bar{q}=\frac{1}{2\pi aR(\psi_2-\psi_1)}\int_0^{2\pi}\int_{\psi_1}^{\psi_2}q(R+a\sin\theta)a\,d\psi\,d\theta. \quad (5)$$

In the region of fully developed temperature profiles, equation (5) simplifies to

$$\bar{q}=\frac{1}{2\pi(R/a)}\int_0^{2\pi}q(R/a+\sin\theta)d\theta. \quad (6)$$

By introducing the defining equation for the heat-transfer coefficient, $h\equiv q/(T_w-T_m)$, equation (6) can be put in the form,

$$\overline{Nu}=\frac{2\bar{h}a}{k}=\frac{1}{2\pi(R/a)}\int_0^{2\pi}Nu(R/a+\sin\theta)d\theta. \quad (7)$$

It is well known that, in the region of fully developed temperature profiles under axially uniform wall-heat-flux conditions, a constant-axial-temperature gradient is established at every point in the tube cross section. The relationship between this gradient and the averaged heat flux at the wall is established by a heat balance on the fluid, such that

$$\frac{\partial T}{\partial\psi}=\frac{dT_w}{d\psi}=\frac{dT_m}{d\psi}=\frac{2R\bar{q}}{w_m\rho ac_p}=\frac{4(R/a)a\bar{q}}{k\,Re\,Pr}\text{ and }\frac{\partial^2 T}{\partial\psi^2}=0. \quad (8)$$

It is convenient to introduce the dimensionless temperatures, H and ϕ, defined as

$$H = \frac{(T_w - T)(R/a)}{Re\,Pr\,dT_m/d\psi} \text{ and } \phi = \frac{T_w - T}{T_w - T_m}. \quad (9)$$

It should be noted that ϕ can also be expressed as H/H_m. By means of equations (8) and the dimensionless temperature, H, equation (3) can be put in the following dimensionless form:

$$\frac{\partial^2 H}{\partial \eta^2} + \frac{1}{\eta^2}\frac{\partial^2 H}{\partial \theta^2} + \left(\frac{1}{\eta} + \frac{\sin\theta}{R/a + \eta\sin\theta} - Pr\,U\right)\frac{\partial H}{\partial \eta} + \left(\frac{\cos\theta}{\eta(R/a + \eta\sin\theta)} - Pr\frac{V}{\eta}\right)\frac{\partial H}{\partial \theta} + \frac{W(R/a)}{(R/a + \eta\sin\theta)Re} = 0. \quad (10)$$

The boundary condition for equation (10) is $H = 0$ at the wall of the tube.

An expression for the local Nusselt number in terms of the dimensionless temperature field can be found by considering the following expression for the local heat flux at the wall:

$$q = k\left(\frac{\partial T}{\partial r}\right)_{r=a} = h(T_w - T_m). \quad (11)$$

In terms of the dimensionless temperature, equation (11) can be expressed as

$$Nu = \frac{2ha}{k} = \frac{-2(\partial H/\partial \eta)_{\eta=1}}{H_m} = -2\left(\frac{\partial \phi}{\partial \eta}\right)_{\eta=1}. \quad (12)$$

An expression for the peripherally averaged Nusselt number can be found by considering the overall heat balance expressed in equations (8); i.e.

$$\frac{dT_m}{d\psi} = \frac{4(R/a)a\bar{q}}{k\,Re\,Pr} = \frac{4(R/a)a\bar{h}(T_w - T_m)}{k\,Re\,Pr}. \quad (13)$$

In terms of the dimensionless temperature, H, equation (13) becomes

$$\overline{Nu} = \frac{2\bar{h}a}{k} = \frac{1}{2H_m}, \quad (14)$$

where H_m is the flow-averaged mean value of H over the flow cross section and is defined by the relationship,

$$H_m = \frac{1}{W_m \pi}\int_0^{2\pi}\int_0^1 W H \eta\, d\eta\, d\theta = \frac{2}{\pi Re}\int_0^{2\pi}\int_0^1 W H \eta\, d\eta\, d\theta. \quad (15)$$

METHOD OF NUMERICAL SOLUTION FOR TEMPERATURE FIELDS

Because of its symmetry, only half of the tube cross section need be considered in a numerical solution. The finite-difference grid used for the solution of the temperature field was the same as that used in Austin's solution [1] of the flow problem. Radial and angular ($\theta = -\pi/2$ to $\theta = \pi/2$) directions were divided into twenty equal intervals. Solution of the flow problem by the method described by Austin [1] yields the three velocity components, U, V and W, at each of the grid points. The dimensionless thermal-energy equation, equation (10), can be put in finite-difference form by employing standard first-central-difference operators for the first and second partial derivatives in both the radial and angular directions. Equation (10) the interior grid points, with the exception of the center point, which is on the center line of the tube. Since equation (10) is singular there, a special equation, based on symmetry conditions, was provided for the center point.

Boundary conditions for the semicircular region are:

$H = 0$, $\eta = 1$ (solid wall); (16a)

$\partial H/\partial \theta = 0$, $\theta = \pm\pi/2$ (symmetry); (16b)

$\partial H/\partial \eta = 0$, $\theta = 0$, $\eta = 0$ (symmetry). (16c)

The above discretization procedure yields a set of 400 linear equations in the 400 unknown temperatures at the interior grid points. A point successive-overrelaxation (S.O.R) method was

used to solve this set of equations. A complete discussion of this method is given by Young [17]. The S.O.R. method, as utilized here, involves use of a relaxation factor, $0 < \omega < 2$, intended to speed the rate of convergence. For a given set of parameters, it was discovered that increasing the relaxation factor led to faster convergence until a point was reached where the numerical solution diverged. The maximum value of ω for which convergence occurred was shifted to smaller values as the Prandtl and Dean numbers were increased. Although very small relaxation factors were required for some runs, the range of results reported in this study was not limited by convergence problems but by decreasing accuracy as very large values of the Prandtl and Dean numbers were reached.

Iteration was terminated when the following relative-error criterion was satisfied:

$$\max \left| H_{I,J}{}^{n} - H_{I,J}{}^{n-1} \right| / H_{I,J}{}^{n} < \varepsilon, \quad (17)$$

where ε is a prescribed convergence criterion. An ε of 10^{-6} was used for about 95 per cent of the numerical runs, with ε of 10^{-5} being used for the remaining runs. Numerical experiment showed no significant difference in results for these two criteria. Calculations were performed on a Univac 1108 digital computer. An initial approximation for the iterative calculations could be supplied either from the results of a previous run or from an approximate solution obtained by directly solving a set of 122 equations for a coarse mesh. The number of complete passes (iterations) through the 400 equations required to satisfy the convergence criterion varied greatly, generally increasing with higher Prandtl and Dean numbers. The required set of iterations varied from about one hundred to several thousand and took from as little as 3 s to about $1\frac{1}{2}$ min of computation time.

To provide one check of the accuracy of the numerical solution, calculations were performed using known straight-tube velocity profiles and a value of 10^{16} for R/a, which approximates the infinite curvature of a straight tube. The results of these calculations for two straight-tube velocity profiles are shown in Table 1. The calculated temperature fields for these two cases were axially symmetric, as expected.

Table 1. Numerically calculated Nu *for straight tubes*

Calculation method	Plug flow	Laminar (Poiseuille)
Exact	8	$48/11 \cong 4{\cdot}364$
Numerical	8·0000	4·358

Another check on the accuracy of the numerical solution was made. Combining equations (7) and (12) and restating equation (14), we have

$$\overline{Nu} = \frac{-1}{\pi(R/a)} \int_{0}^{2\pi} \left(\frac{\partial \phi}{\partial \eta} \right)_{\eta=1} (R/a + \sin\theta) \mathrm{d}\theta$$

$$\text{and } \overline{Nu} = \frac{1}{2H_m}. \quad (18)$$

Equations (18) constitute two independent means of calculating the average Nusselt number from the numerical data. The single integral in equations (18) and the double integral in equation (15) for H_m are evaluated numerically by one- and two-dimensional Simpson's rules, respectively. The percentage difference in the two estimates of $\overline{Nu}$ is taken as a measure of error for solution of the thermal-energy equation, assuming the velocity profiles are exact. All average Nusselt-number results reported here are based on the second of equations (18). For 126 runs, covering a Dean-number range of 1–1200 and a Prandtl-number range of 0·005–1600, the error in the heat-transfer results predicted by equations (18) is 0·7, 1·0 and 3·0 per cent, respectively, for the average, standard, and maximum deviations.

It is shown by Austin [1] that the following

relationships hold for the ratio of curved-to-straight-tube friction factors:

$$\frac{f_c}{f_s} = \frac{-1}{4\pi\, Re(R/a)} \int_0^{2\pi} \left(\frac{\partial W}{\partial \eta}\right)_{\eta=1} (R/a + \sin\theta)\mathrm{d}\theta$$

$$\text{and} \quad \frac{f_c}{f_s} = \frac{-\partial P/\partial Z}{4\, Re}, \qquad (19)$$

where f_s is the Fanning friction factor for straight tubes ($f_s = 16/Re$) and f_c is the corresponding factor for curved tubes. These two independent relationships can be used to estimate the error in the velocity profiles. For the 25 sets of velocity profiles used in this study, the error predicted by equations (19) is 1·4, 2·2 and 5·5 per cent, respectively, for the average, standard, and maximum deviations. The maximum deviation occurred for the run at a Dean number of 1200—the highest Dean number investigated.

Comparison of the predicted errors indicates that, for the range of parameters studied here, the accuracy of the heat-transfer results is limited by the accuracy of the velocity profiles. Therefore, except for the very high Dean-number region, the numerical heat-transfer results appear to be accurate to within two per cent.

DISCUSSION OF TEMPERATURE PROFILES

An isometric representation of the dimensionless temperature, ϕ, is shown in Figs. 3 and 4 for Prandtl numbers of 0·7 and 5, respectively, for a Dean number of 714 and a curvature of 15·2. Points of maxima on these figures correspond to points of lowest or highest fluid temperature, depending on whether heating or cooling, respectively, is being considered.

Figure 3, for a Prandtl number of 0·7, shows that the temperature profile is skewed toward

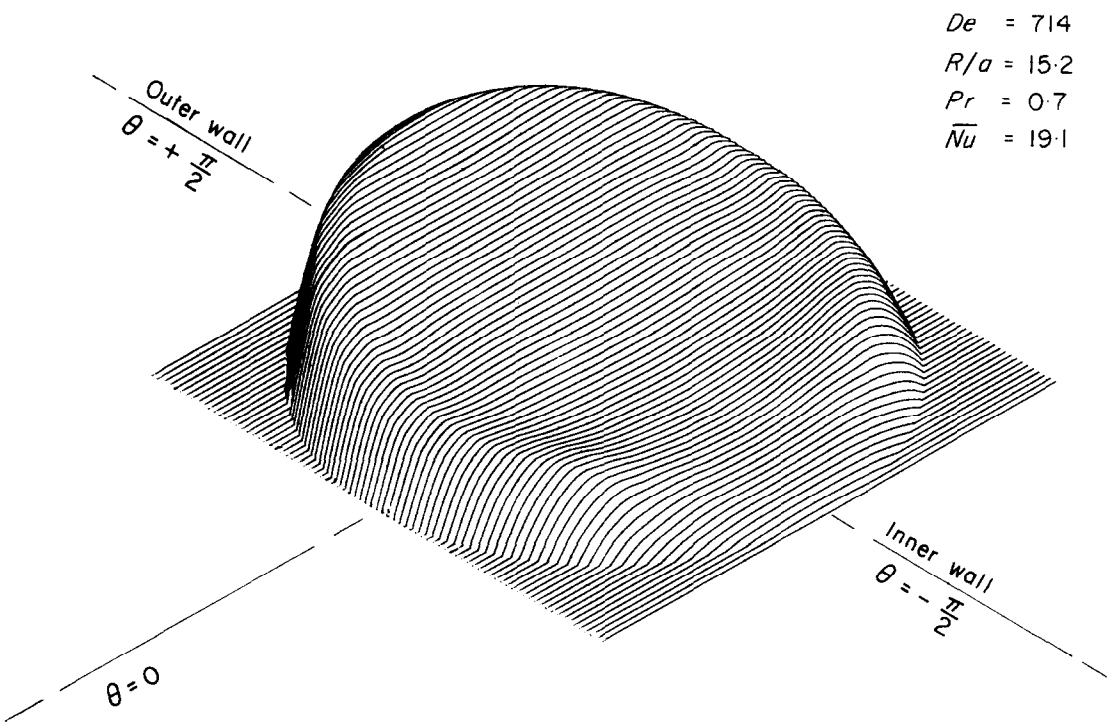

FIG. 3. Dimensionless temperature, $Pr = 0{\cdot}7$, $De = 714$, $R/a = 15{\cdot}2$.

the outer wall. The maximum dimensionless temperature in Fig. 3 occurs at a point near the outer wall on the diameter of symmetry, extending from $\theta = -\pi/2$ to $\theta = +\pi/2$. The radial-temperature gradient at the wall in the vicinity of the outer wall is seen to be large, and it increases with increasing Dean number. The radial-temperature gradient at the wall in the vicinity of the inner wall, however, is quite small and is usually less than the value attained in a straight tube.

For Prandtl numbers greater than 1, the temperature field is much different. Equation (3), the thermal-energy equation, indicates that, as the Prandtl number is increased, the convective fluxes on the left-hand side of the equation increase in magnitude and importance relative to the diffusive fluxes on the right-hand side of the equation. Figure 4, which illustrates the effect of higher Prandtl numbers on the temperature field, shows that the point of maximum dimensionless temperature has been shifted off the axis of symmetry, causing double maxima to appear. A sloping depression in the temperature field runs across the center of the tube. The magnitude of the dimensionless temperature along the floor of this depression decreases i.e. approaches the wall temperature more closely, as either the Prandtl number is increased or the secondary circulation is increased by increasing the Dean number. Either of these changes increases the magnitude of the secondary convective fluxes. A considerable portion of the fluid in the vicinity of the inner wall is at temperatures not far removed from the wall temperature. This is a result of the secondary flow entering the central region in the vicinity of the inner wall. This fluid has just passed along streamlines running close to the wall from the outer wall all the way back to

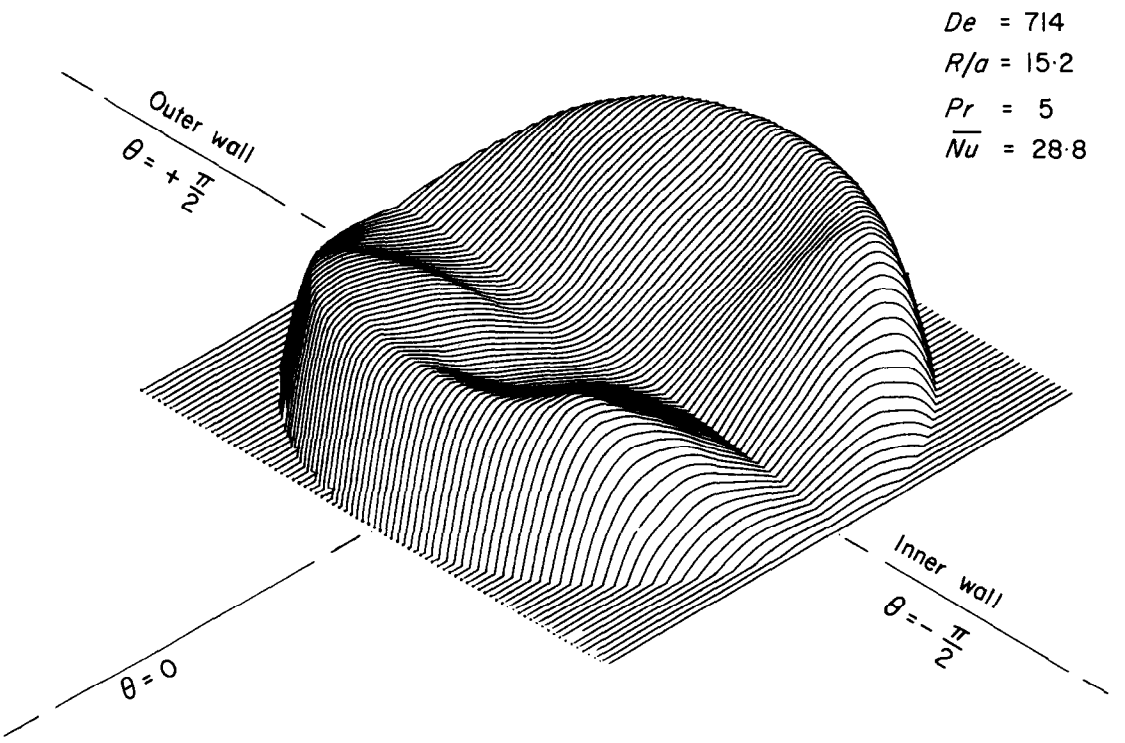

FIG. 4. Dimensionless temperature, $Pr = 5$, $De = 714$, $R/a = 15{\cdot}2$.

the inner wall and, as a result, has been heated (or cooled) close to the wall temperature. This region of low dimensionless temperature is then propagated across the center of the tube by the secondary flow. For higher Prandtl numbers, diffusive fluxes are less effective in smoothing out and dispersing this propagated region of low dimensionless temperature; consequently, a deep depression can exist across the entire temperature field.

The type of temperature profile shown in Fig. 4 was also obtained by Dravid *et al.* [3, 14] in their numerical calculations at a Dean number of 225, using the approximate velocity profiles obtained by Mori and Nakayama [9]. Also, Fig. 4 is in qualitative agreement with the exploratory measurements made by Hawes [11], using water.

For low-Prandtl-number fluids, such as liquid metals, diffusive-energy fluxes have a greater influence on the temperature field than do convective fluxes; and no depression develops in the temperature field, even when the secondary circulation is very strong.

The constant-property species-conservation equation, without chemical reaction and with only ordinary diffusion, is exactly analogous to the constant-property thermal-energy equation as presented in equation (3), but with concentration instead of temperature and a Schmidt number ($Sc \equiv \nu/D$) instead of the Prandtl number. With the assumptions of small mass-transfer rates—so as not to affect the velocity profiles appreciably—and similar boundary conditions, the results presented here are exactly applicable to mass transfer in curved tubes. The analogous boundary condition for mass transfer would be axially uniform wall mass flux with peripherally uniform wall concentration. Curved-tube effects are particularly important for high-Schmidt-number fluids.

TRANSPORT FACTORS

The numerically calculated Nusselt numbers for the low-Dean-number region are compared with the perturbation solution of Özisik and Topakoglu [15] in Fig. 5. Each of the perturbation-solution curves for a given Prandtl number represents many different curves for various curvatures which, if drawn, would have been indistinguishable from the single curve shown.*

The experimental work of Mori and Nakayama [9] and of Dravid *et al.* [3, 14] approaches closely the boundary condition used in this numerical study. Both investigators used electrically heated tubes having relatively thick walls of relatively high thermal conductivity. The numerically calculated average Nusselt numbers are compared with these experimental data in Fig. 6. Mori and Nakayama's measurements, using air ($Pr = 0{\cdot}7$), are in good agreement with the numerical results. Dravid *et al.* made measurements of the local, peripherally averaged Nusselt number for five liquids having Prandtl numbers ranging from about 5 to about 200. Their data for the two liquids having the lowest and highest Prandtl numbers—water and ethylene glycol, respectively—are shown in Fig. 6. Their experimental results for the fully developed, average Nusselt number are subject to two sources of error: (1) the oscillations in their experimental measurements, which had been predicted in their numerical study, sometimes did not damp out completely by the end of the tube; in these cases, extrapolation to the fully developed values must have involved considerable subjective error; and (2) property variations caused the Prandtl number to vary as much as 33 per cent from the tube inlet to its outlet, and the estimated fully developed Nusselt numbers were associated with a Prandtl number based on the mean of

* It should be mentioned that the Reynolds number in [15] is based on the mean velocity in a straight tube with the same diameter and with the same axial-pressure gradient as that of a curved tube, whereas the Reynolds number in this paper is based on the mean velocity in the curved tube. The conversion factor between these two definitions is simply the ratio of mass-flow rates for the straight and curved tubes. This ratio, given analytically [15], was used to make the comparison in Fig. 5 consistent with the definitions used in this paper. This conversion factor was significantly different from a value of one only at Dean numbers greater than ten.

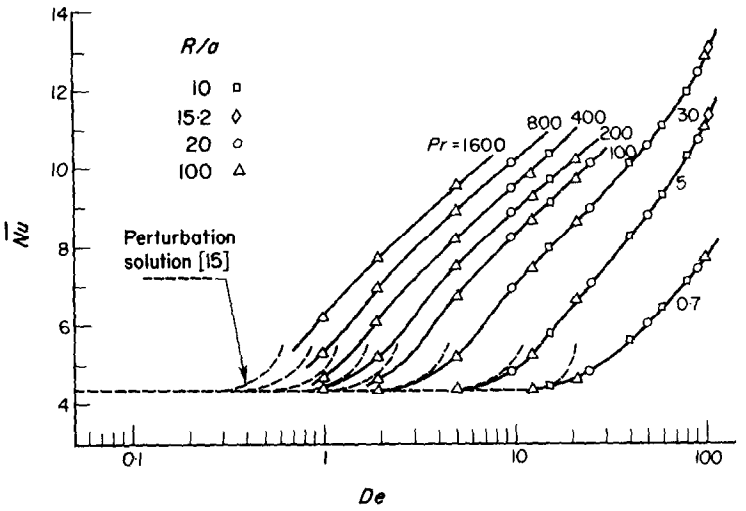

FIG. 5. Comparison of numerical results with perturbation solution at low Dean numbers.

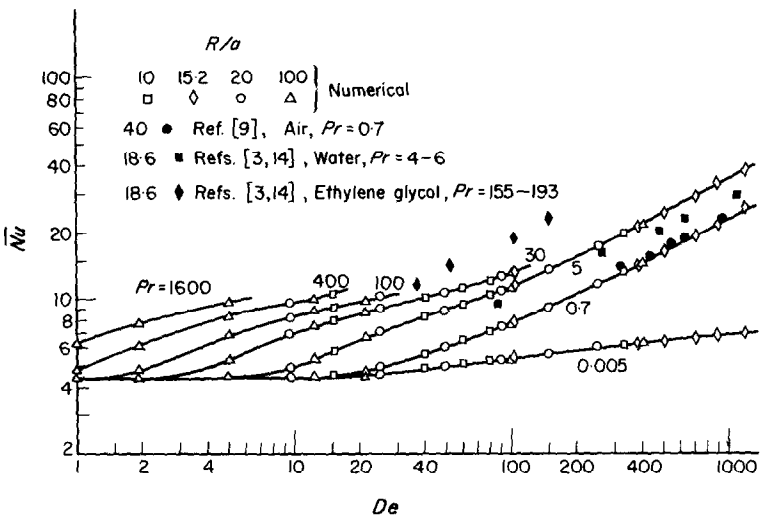

FIG. 6. Comparison of numerical results with experimental data in literature.

the inlet and outlet temperatures. Since they extrapolated their data near the outlet of the tube to estimate the fully developed Nusselt number, it would seem more correct to base the results on the Prandtl number at the tube outlet, which was always lower than the Prandtl number at the tube inlet. This might explain why their data for water ($Pr = 4$ at outlet, $Pr = 6$ at inlet) fall below the numerical results for $Pr = 5$. Despite these problems, their data are in fair accord with the numerical results.

Figures 5 and 6 indicate that the curvature

parameter, in the range of 10–100, has a negligible effect on the average Nusselt number, as all numerical data for a given Prandtl number fall on a single curve. However, the curvature parameter has a definite effect on the peripheral variation of the fully developed local Nusselt number. Figure 7 shows this effect for two flow

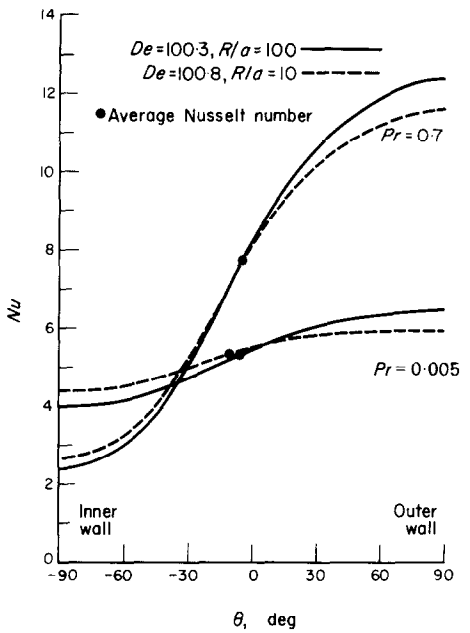

FIG. 7. Effect of curvature parameter, R/a, above that expressed in the Dean number, $Re\sqrt{a/R}$.

situations having very nearly the same Dean number but curvatures of 10 and 100. The data shown for Prandtl numbers of 0·005 and 0·7 indicate that increasing the curvature while maintaining a constant Dean number increases the spread in the local Nusselt numbers from inner to outer walls. This effect of curvature is not a large one, however; and it appears to become less noticeable at higher Prandtl numbers.

Figures 8 and 9 show the effect of the Dean number on the peripheral variation in the fully developed Nusselt number for Prandtl numbers of 0·7 and 5, respectively. These figures indicate that, as the Dean number is increased, a

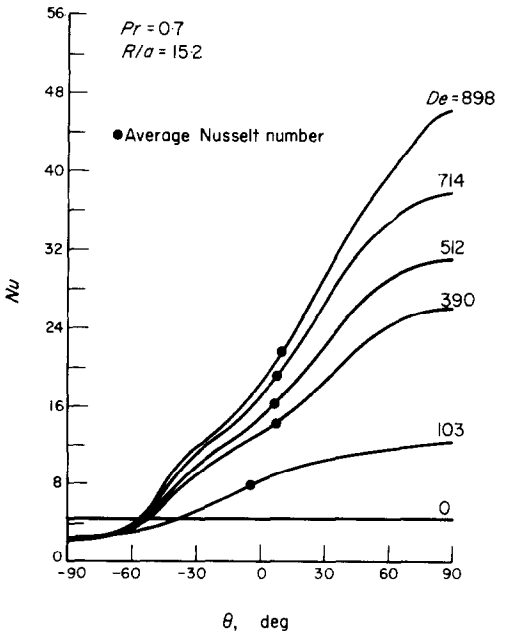

FIG. 8. Peripheral variation of fully developed Nusselt number, $Pr = 0{\cdot}7$.

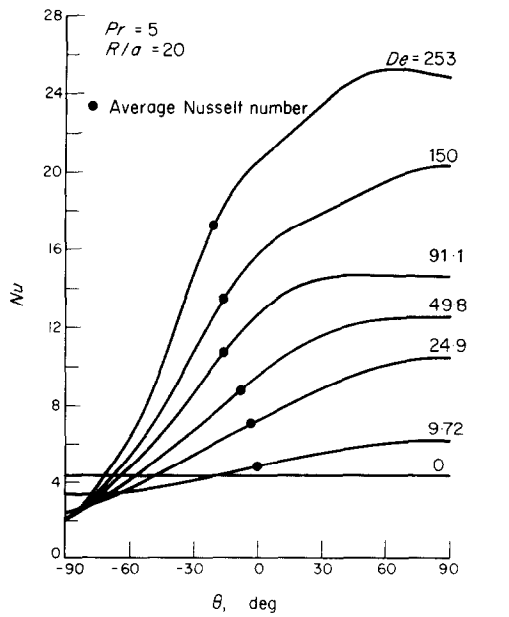

FIG. 9. Peripheral variation of fully developed Nusselt number, $Pr = 5$.

greater proportion of the heat being supplied to the tube wall is being conducted within the wall and is entering the fluid in the vicinity of the outer wall. It was observed that, for Prandtl numbers of 0·7 and greater, the local Nusselt number in the immediate vicinity of the inner wall was always less than the Nusselt number for a straight tube; i.e. 48/11. This can be explained by recalling that the fluid in the vicinity of the inner wall is at temperatures relatively close to the wall temperature due to the secondary flow which has passed near the wall and has been heated (or cooled) close to the wall temperature. This effect increases as the Dean number (and, therefore, the secondary flow) is increased, causing the Nusselt number at the inner wall to decrease until a limiting value is apparently reached. The local Nusselt numbers at the outer regions of the wall, however, continue to increase as the Dean number is increased. In general, high Prandtl numbers tend to give local Nusselt numbers which are more uniformly high over a relatively large section of the tube, extending from the outer wall back to near the inner wall, where a pronounced minimum occurs. For Prandtl numbers of 0·7 and less, however, the distribution tends to increase much more uniformly from inner to outer walls. For Prandtl numbers greater than 0·7 and large Dean numbers, the maximum local Nusselt number sometimes occurred at a point on the wall between $\theta = 0$ and $\theta = +\pi/2$; for Prandtl numbers of 0·7 or less, however, the maximum always occurred at $\theta = +\pi/2$. The numerical results for high Prandtl numbers are in qualitative agreement with the approximate measurements of local Nusselt numbers made by Seban and McLaughlin [12], using an oil. A correlation for the ratio of local Nusselt numbers at outer and inner walls is presented in Fig. 10.

RECOMMENDED DESIGN CORRELATIONS

The results reported here should prove useful in the design of many types of heat- and mass-transfer devices and non-adiabatic reactors employing curved circular passages. Heat- and mass-transfer coefficients in such devices can be much larger than those obtained in straight tubes. Also, the secondary flows caused by centrifugal forces stabilize the flow such that critical Reynolds numbers for transition to turbulent flow are much higher for curved tubes. The critical Reynolds number for curved tubes

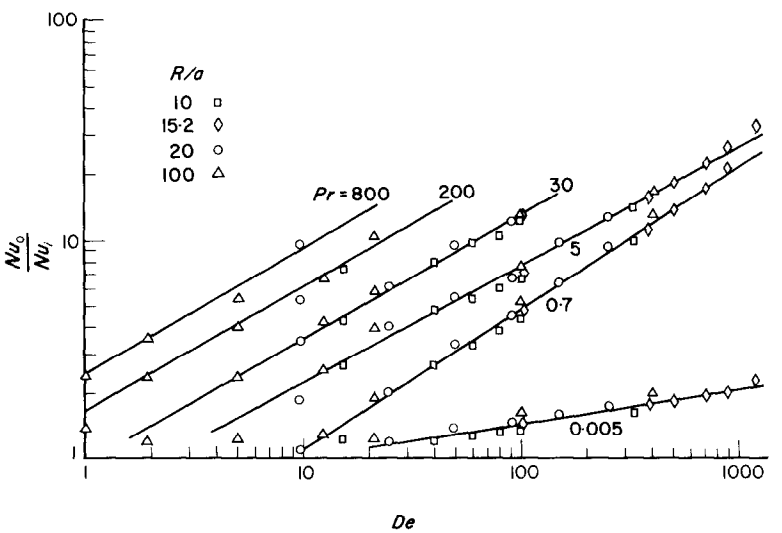

FIG. 10. Ratio of local Nusselt numbers at outer and inner wall.

increases as the curvature, R/a, is decreased. The following empirical equation, proposed by Srinivasan *et al.* [18],

$$Re_c = 2100\left(1 + \frac{12}{\sqrt{R/a}}\right), \qquad (20)$$

can be used to estimate curved-tube critical Reynolds numbers for curvatures as low as 10. A lower practical limit for the curvature parameter in most devices would probably be about 5. Assuming that the critical Reynolds number for a curvature of 5 is at least 10000 (the critical value for a curvature of 10 as predicted by equation (20)), one can calculate that Dean numbers as large as 4500 are of practical importance in the viscous-flow regime.

Frictional losses for curved tubes are higher than those for straight tubes. The fractional increase in heat- (mass-) transfer coefficients relative to the fractional increase in friction factors for curved and straight tubes is shown in Fig. 11, where the numerically calculated

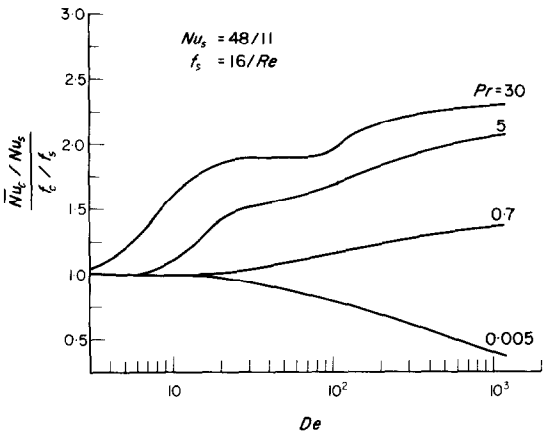

FIG. 11. Efficiency of curved tubes relative to straight tubes.

friction factors and average Nusselt numbers were used to derive the curves shown. The curve for a Prandtl number of 30 was extended beyond a Dean number of 100 by use of the empirical correlation discussed below for the fully developed Nusselt number proposed by Dravid *et al.* [3, 14]. The unusual shape of the curves for Prandtl numbers of 5 and 30 result from the several inflections evident in the average-Nusselt-number data shown in Fig. 6. It should be noted that, except for liquid metals ($Pr = 0{\cdot}005$), the fractional increase in heat- (mass-) transfer coefficients is significantly greater than the fractional increase in friction losses. For high Prandtl numbers, this enhancement relative to straight tubes is most significant.

Dravid *et al.* [3, 14] recommend the following empirical correlation for the fully developed Nusselt number, applicable for Dean numbers between 50 and 2000 and for Prandtl numbers between 5 and 175:

$$\overline{Nu} = [0{\cdot}65\sqrt{De} + 0{\cdot}76]Pr^{0{\cdot}175}. \qquad (21)$$

This equation is based on their estimate of the fully developed Nusselt number obtained by extrapolating local, peripherally averaged, Nusselt-number data for five liquids. Equation (21) is in reasonable agreement with the extrapolated numerical results of this study at high Prandtl numbers. A graphical correlation for the fully developed Nusselt number, covering all Dean numbers of practical interest and Prandtl numbers from 0·005 to 1600, is presented in Fig. 12. This correlation is based on the numerical data shown in Fig. 6 and equation (21). The regions where interpolation was used between these two correlations are also shown. It should be noted that, in Fig. 12, equation (21) was used at higher Prandtl numbers than were

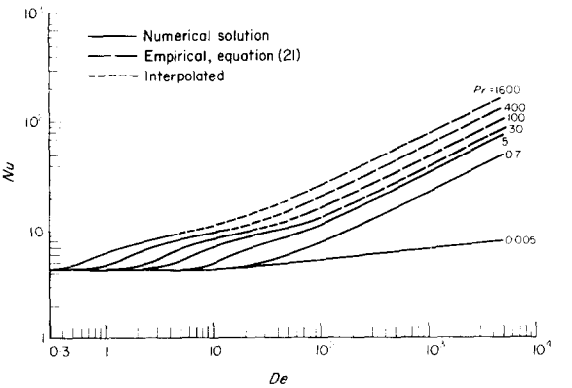

FIG. 12. Graphical design correlation for fully developed Nusselt number.

used in the experimental work on which equation (21) is based; accordingly, the curves for $Pr = 400$ and 1600 are tentative in the high-Dean-number region.

The numerical data were analyzed by least-squares techniques to provide equations showing the effects of the Prandtl number and the Dean number on the Nusselt number. The numerical results in the low-Prandtl-number range were correlated by the equation,

$$\overline{Nu} = 3{\cdot}31\, De^{0{\cdot}115}\, Pr^{0{\cdot}0108},\ 20 \leqslant De \leqslant 1200,\quad 0{\cdot}005 \leqslant Pr \leqslant 0{\cdot}05, \qquad (22)$$

with a standard deviation of 1·4 per cent and a maximum deviation of 4 per cent. The data for a Prandtl number of 0·05 were only slightly higher than those for a Prandtl number of 0·005; hence, the low exponent on the Prandtl number in equation (22).

The numerical results for Prandtl numbers in the range of 0·7–5 were correlated by the equation,

$$\overline{Nu} = 0{\cdot}913\, De^{0{\cdot}476}\, Pr^{0{\cdot}200},\ 80 \leqslant De \leqslant 1200,\quad 0{\cdot}7 \leqslant Pr \leqslant 5, \qquad (23)$$

with a standard deviation of 2·3 per cent and a maximum deviation of 5 per cent. The numerical results for Prandtl numbers of both 0·7 and 5 for Dean numbers greater than about 250 confirm the 0·5 power on the Dean number predicted at large Dean numbers by Mori and Nakayama [9]. However, when fitting data for Dean numbers as low as 80 to equations of the form of equation (23), the exponent on the Dean number is determined to be 0·476. A least-squares analysis of the data of Dravid *et al.* [3, 14] was made. When cast in the form of equation (23), their data yield a Dean-number exponent of about 0·47, in good agreement with the numerical results of this study.

CONCLUDING REMARKS

1. Fully developed heat transfer to viscous flow in curved circular tubes was studied theoretically for the boundary condition of axially uniform wall heat flux with peripherally uniform wall temperature. Numerical results are not limited to slightly curved tubes nor to small Dean numbers.

2. Design correlations are presented for the fully developed Nusselt number with Dean numbers covering the entire range of practical interest and Prandtl numbers of 0·005–1600. Detailed information on the variation in transport coefficients around the periphery of a tube is presented. The curvature parameter, R/a, in the range of 10–100, was found to have a negligible influence on the average Nusselt number. However, the curvature parameter has a small effect on the peripheral variation of transport coefficients. Use of fully developed Nusselt numbers in design is expected to be only slightly conservative, as the fully developed region is approached rapidly in curved tubes [12, 14].

3. The results are directly applicable to mass transfer in the absence of chemical reaction and with ordinary diffusion and should find application to problems of bioengineering interest. Very large increases in mass-transfer coefficients over those attained in straight tubes are predicted for mass transfer in liquids, where Schmidt numbers of the order of 1000 and greater commonly occur.

ACKNOWLEDGEMENTS

This research was supported primarily through a National Aeronautics and Space Administration Traineeship in the Chemical Engineering Department at the University of Utah. The authors wish to acknowledge the contributions of Dr. L. R. Austin, who provided the computer program for the calculation of velocity profiles in curved tubes and the program used for preparing the isometric plots.

REFERENCES

1. L. R. Austin, The development of viscous flow within helical coils, Ph.D. Thesis, University of Utah, Salt Lake City, Utah (1971).
2. M. H. Weissman and L. F. Mockros, Gas transfer to blood flowing in coiled circular tubes, *A.S.C.E. Proc., Eng. Mech. Div. Jl* **94**, 857–872 (1968).
3. A. N. Dravid, The effect of secondary fluid motion on laminar flow heat transfer in helically coiled tubes, Sc.D. Thesis, Massachusetts Institute of Technology, Cambridge, Massachusetts (1969).

4. W. R. DEAN, Note on the motion of fluid in a curved pipe, *Phil. Mag.* **4**, 208–223 (1927).
5. W. R. DEAN, The stream-line motion of fluid in a curved pipe, *Phil. Mag.* **5**, 673–695 (1928).
6. H. C. TOPAKOGLU, Steady laminar flows of an incompressible viscous fluid in curved pipes, *J. Math. Mech.* **16**, 1321–1337 (1967).
7. M. ADLER, Strömung in gekrümmten rohren, *Z. Angew. Math. Mech.* **14**, 257–275 (1934).
8. S. N. BARUA, On secondary flow in stationary curved pipes, *Q. J. Mech. Appl. Math.* **16**, 61–77 (1963).
9. Y. MORI and W. NAKAYAMA, Study on forced convective heat transfer in curved pipes (1st report, laminar region), *Int. J. Heat Mass Transfer* **8**, 67–82 (1965).
10. L. C. TRUESDELL, JR. and R. J. ADLER, Numerical treatment of fully developed laminar flow in helically coiled tubes, *A.I.Ch.E. Jl* **16**, 1010–1015 (1970).
11. W. B. HAWES, Some sidelights on the heat transfer problem, *Trans. Instn Chem. Engrs* **10**, 161–167 (1932).
12. R. A. SEBAN and E. F. MCLAUGHLIN, Heat transfer in tube coils with laminar and turbulent flow, *Int. J. Heat Mass Transfer* **6**, 387–395 (1963).
13. Y. MORI and W. NAKAYAMA, Study on forced convective heat transfer in curved pipes (3rd report, theoretical analysis under the condition of uniform wall temperature and practical formulae), *Int. J. Heat Mass Transfer* **10**, 681–695 (1967).
14. A. N. DRAVID, K. A. SMITH, E. W. MERRILL and P. L. T. BRIAN, Effect of secondary fluid motion on laminar flow heat transfer in helically coiled tubes, *A.I.Ch.E. Jl* **17**, 1114–1122 (1971).
15. M. N. ÖZISIK and H. C. TOPAKOGLU, Heat transfer for laminar flow in a curved pipe, *J. Heat Transfer* **90**, 313–318 (1968).
16. H. MAEKAWA, Heat transfer to fully developed laminar flow in a gently curved pipe, Preprint of 1st Japan Heat Transfer Symposium, p. 13 (1964).
17. D. YOUNG, The numerical solution of elliptic and parabolic partial differential equations, *Survey Of Numerical Analysis*, edited by J. TODD, pp. 380–438. McGraw-Hill, New York (1962).
18. P. S. SRINIVASAN, S. S. NANDAPURKAR and F. A. HOLLAND, Pressure drop and heat transfer in coils, *Chem. Engr* No. 218, 113–119 (1968).

PHÉNOMÈNES DE TRANSFERT THERMIQUE ET MASSIQUE POUR UN ÉCOULEMENT VISQUEUX DANS DES TUBES CIRCULAIRES COURBES

Résumé—On a étudié théoriquement le transfert thermique pour un écoulement permanent visqueux dans des tubes courbes de section droite circulaire, pour des champs de température et de vitesse entièrement développés sous les conditions aux limites de flux pariétal uniforme longitudinalement et de température pariétale uniforme périphériquement. Les profils de vitesse entièrement développés utilisés ici ont été calculés par une méthode numérique rigoureuse [1]. L'équation d'énergie thermique a été résolue numériquement par utilisation d'une méthode de surrelaxation successive. Les résultats ne sont pas limités à des tubes légèrement courbes et des nombres de Dean bas, comme dans les analyses précédentes. Des solutions sont présentées pour un domaine du nombre de Dean compris entre 1 et 1200. On a fait varier le nombre de Prandtl de 0,005 à 1600 et les paramètres de courbure de 10 à 100. Le nombre de Nusselt moyen sur la périphérie peut être formulé comme une fonction des nombres de Dean et de Prandtl seulement; mais, quand on considère la variation du nombre de Nusselt local sur la périphérie, le rapport de courbure entre comme un paramètre additionnel.

WÄRME- UND STOFFÜBERTRAGUNGSPHÄNOMENE FÜR EINE VISKOSE STRÖMUNG IN GEKRÜMMTEN KREISFÖRMIGEN ROHREN

Zusammenfassung- Die Wärmeübertragung an eine stationäre, viskose Strömung in gekrümmten Rohren mit kreisförmigem Querschnitt wurde für voll ausgebildete Geschwindigkeits- und Temperaturfelder mit der thermischen Randbedingung für axial einheitlichen Wärmestrom mit peripher einheitlicher Wandtemperatur theoretisch untersucht. Die verwendeten, voll ausgebildeten Geschwindigkeitsprofile wurden mittels einer streng numerischen Methode berechnet. Die Wärmeenergiegleichung wurde numerisch unter Benutzung einer punktweise fortlaufenden Überrelaxations-Methode gelöst.

Die Ergebnisse sind nicht wie bei früheren Untersuchnungen auf schwach gekrümmte Rohre und niedrige Dean-Zahlen beschränkt. Für einen Dean-Zahlenbereich von 1 bis 1200 werden Lösungen vorgelegt. Prandtl-Zahlen und Krümmungsverhältnis-Parameter wurden von 0,005 bis 1600, bzw von 10 bis 100 variiert.

Die peripher gemittelte Nusselt-Zahl konnte als eine Funktion allein der Dean- und Prandtl-Zahlen korreliert werden; wird aber eine periphere Variation der Nusselt-Zahl berücksichtigt, tritt das Krümmungsverhältnis als zusätzlicher Parameter auf.

ЯВЛЕНИЯ ТЕПЛО- И МАСООБМЕНА ПРИ ВЯЗКИХ ТЕЧЕНИЯХ В ИСКРИВЛЕННЫХ КРУГЛЫХ ТРУБАХ

Аннотация—Проводится теоретическое исследование переноса тепла при стационарном течении вязких жидкостей в искривленных трубах круглого сечения в случае развитых скоростных и температурных полей при постоянном тепловом потоке с равномерной по окружности трубы температурой стенки. Использованные полностью развитые профили скорости рассчитаны с помощью точного численного метода [1]. Уравнение тепловой энергии решается численно с помощью конечно-разностного метода релаксации. Результаты не ограничиваются искривленными трубами и низкими числами Дина, как в проведенном ранее исследовании. Представленные результаты относятся к диапазону чисел Дина от 1 до 1200. Число Прандтля и параметр кривизны изменяются от 0,005 до 1600 и от 10 до 100 соответственно. Усредненное по окружности число Нуссельта можно обобщить как функцию чисел Дина и Прандтля. Однако, когда рассматривается только изменение числа Нуссельта по окружности, параметр кривизны входит в качестве дополнительного параметра.